Supplementary Information For

Topological nodal line semi-metal with a negative Poisson's ratio in a three-dimensional carbon network with SP^2 hybridization

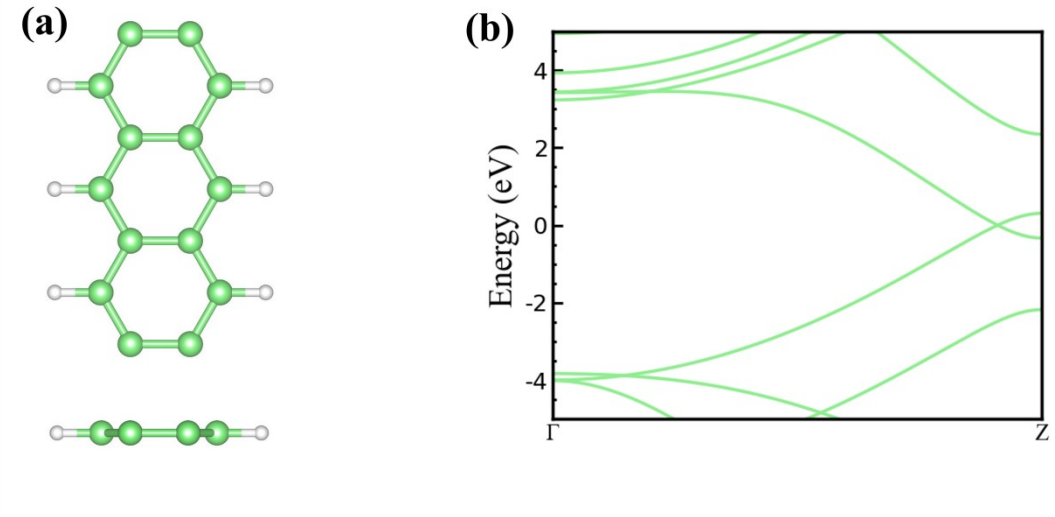

Figure S1. (a) A one-dimensional zigzag graphene nanostrip structure diagram, with edge atoms passivated by hydrogen atoms; (b) The energy band diagram of one-dimensional serrated graphene nanoribbons.

Table S1. Lattice parameters of WZGN.

	Conventional cell	Primitive cell
a	7.76Å	4.03Å
b	3.16Å	4.03Å
c	6.00Å	6.01Å
α	90°	90°
β	90°	90°
γ	90°	131°

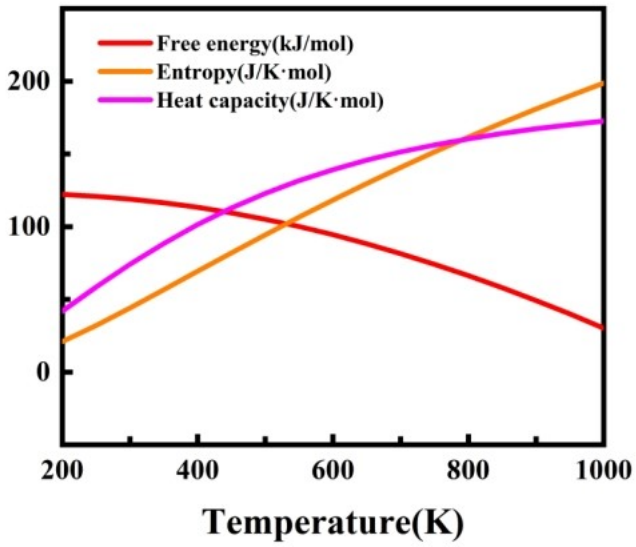

Figure S2 Some thermal properties of WZGN, including Gibbs free energy, entropy, and molar-specific heat capacity in the temperature range of 200K-1000K.

We calculate some thermal properties of WZGN, including Gibbs free energy, entropy, and molar-specific heat capacity in the temperature range of 200K-1000K, as shown in Figure S2. Similar to diamond or graphite, when the temperature is low (e.g., lower than 1000K), the Gibbs free energy almost linearly decreases with temperature [J. Phys. Chem. B 2005, 109, 10435-10440]. However, the value sharply decreases with temperature at high temperature. We suspect that this is associated with the enhancement of anharmonic properties at high temperatures.

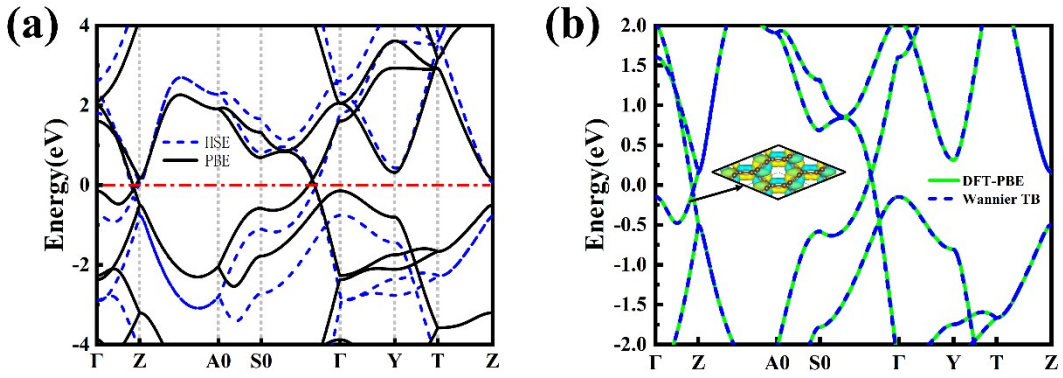

Figure S3. (a) Band structure of WZGN by hybrid functional HSE06 and PBE. The black solid line represents the PBE calculation results, while the blue dashed line represents the HSE06 hybrid functional calculation results. (b) Band structure of WZGN by DFT-PBE and Wannier TB fitting. The green solid line is the result of density functional theory (DFT-PBE) calculation, and the blue dashed line is the result of Wannier TB fitting. The illustration in (b) is the wave function of WZGN (2 × 2 supercells) near the Dirac point.

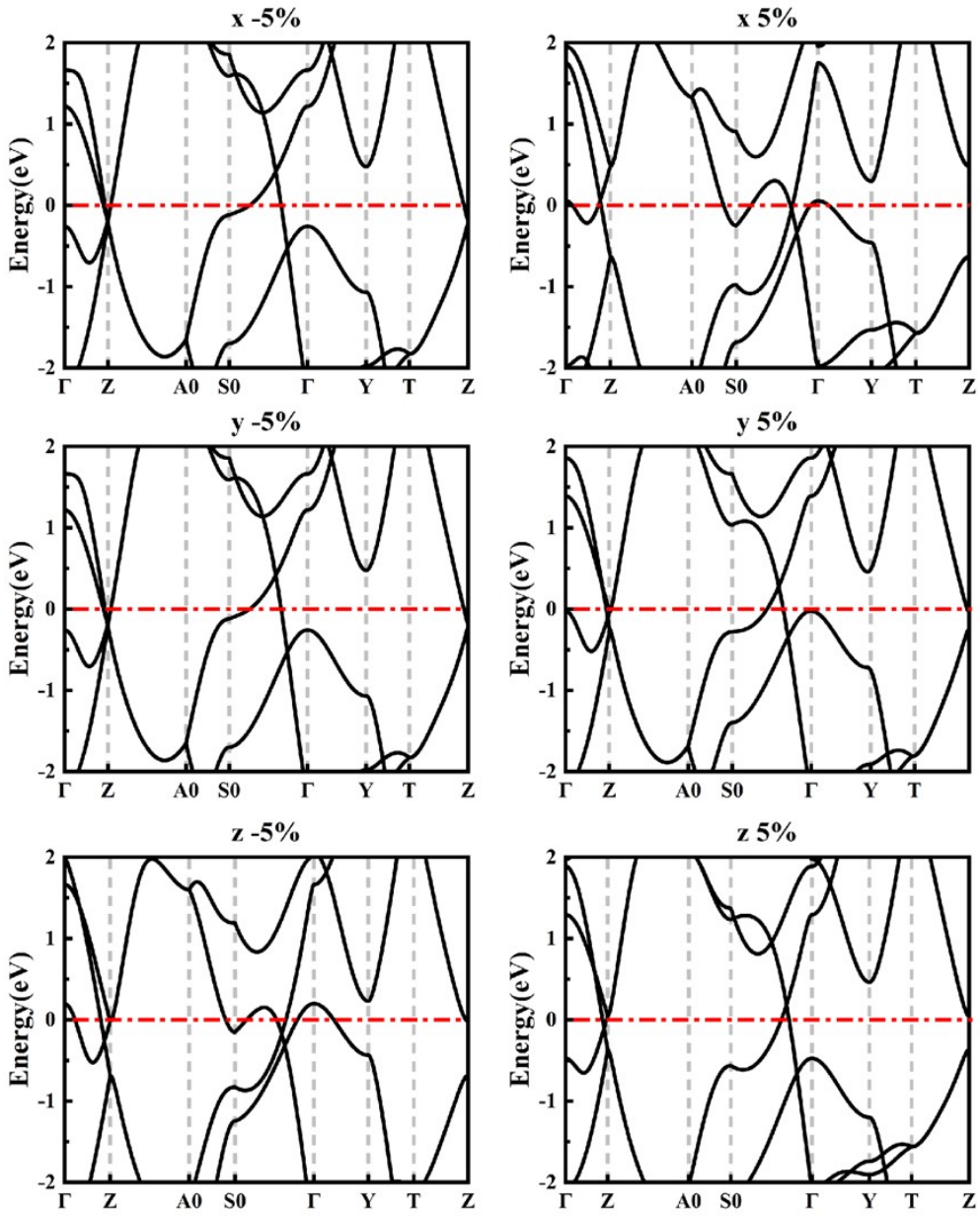

Figure S4 Energy band diagrams after applying 5% uniaxial strain in the *x*, *y*, and *z* directions.

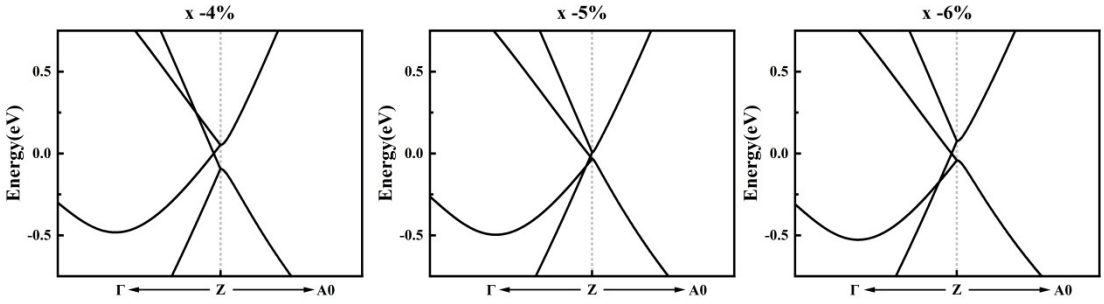

Figure S5 The electronic energy bands near point Z when applying compressive strains of 4%, 5%, and 6% respectively in the *x* direction. Along with this trend of change, we can observe that when a compressive strain of about 5% is applied in the *x* direction, there may be a cross-degeneracy point of four energy bands.

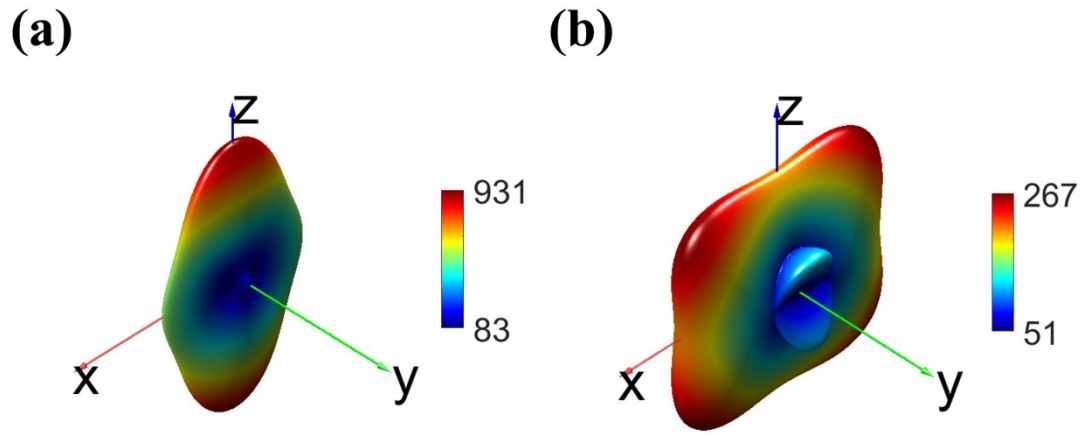

Figure S6. (a) Anisotropic Young's modulus and (b) maximum anisotropic shear modulus of WZGN.

To ensure that our DFT results are appropriate for simulating the strain effect, the molecular dynamic method with the airebo potential function is calculated. As shown in Figure S7(a), the structure breaks when the uniaxial strain is applied to 21.4%, and the maximum value of NPR is about -0.25. Although the structure breaks at 21.4% and the calculated NPR is a bit lower than the DFT, our DFT results and MD simulations are consistent.

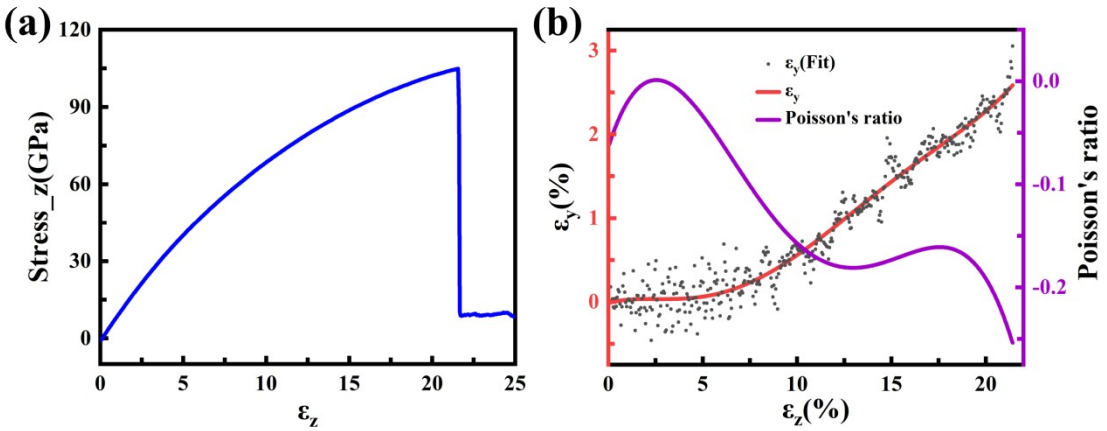

Figure S7. (a) The stress-strain curve in the z-direction, and the curve fractures after 21.4%. (b) Strain Scatter, Fitting Curve, and Poisson's Ratio of WZGN.

Here, one possible synthesis route is proposed. The WZGN can be obtained by stacking twisted two-dimensional carbon structures (e.g., twisted graphene where some bonds are broken), which may be realized by strain engineering in graphene.

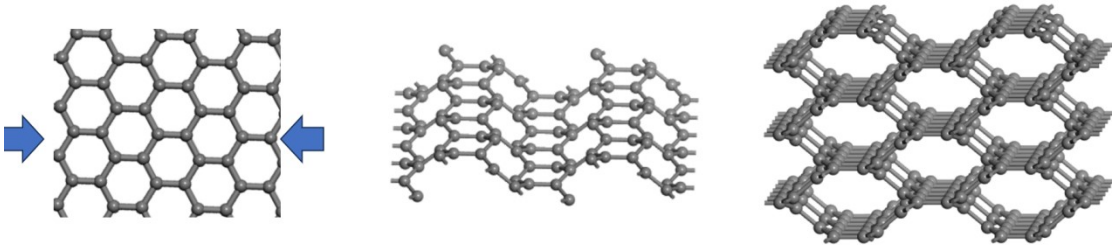

Figure S8. Possible synthesis path for WZGN experiments.